High spatial precision nano-imaging of polarization-sensitive plasmonic particles

Yunbo Liu, Yipei Wang, Somin Eunice Lee

Yunbo Liu, Yipei Wang, Somin Eunice Lee, "High spatial precision nano-imaging of polarization-sensitive plasmonic particles," Proc. SPIE 10506, Nanoscale Imaging, Sensing, and Actuation for Biomedical Applications XV, 105060F (20 February 2018); doi: 10.1117/12.2289143

SPIE.

Event: SPIE BiOS, 2018, San Francisco, California, United States

High spatial precision nano-imaging of polarization-sensitive plasmonic particles

Yunbo Liu, Yipei Wang, Somin Eunice Lee*
Department of Electrical & Computer Engineering, University of Michigan, Ann Arbor, MI 48109,
Department of Biomedical Engineering, University of Michigan, Ann Arbor, MI 48109,
Biointerfaces Institute, University of Michigan, Ann Arbor, MI 48109,
Applied Physics Program, University of Michigan, Ann Arbor, MI 48109

ABSTRACT

Precise polarimetric imaging of polarization-sensitive nanoparticles is essential for resolving their accurate spatial positions beyond the diffraction limit. However, conventional technologies currently suffer from beam deviation errors which cannot be corrected beyond the diffraction limit. To overcome this issue, we experimentally demonstrate a spatially stable nano-imaging system for polarization-sensitive nanoparticles. In this study, we show that by integrating a voltage-tunable imaging variable polarizer with optical microscopy, we are able to suppress beam deviation errors. We expect that this nano-imaging system should allow for acquisition of accurate positional and polarization information from individual nanoparticles in applications where real-time, high precision spatial information is required.

Keywords: plasmonics, optoelectronics, nanophotonics

1. INTRODUCTION

Analyzing individual nanoparticles allows for spatially resolving actual distributions within a heterogeneous population beyond the diffraction limit. Whereas ensemble studies provide a blended average, polarimetric imaging of individual nanoparticles can reveal their orientations.[1–3] By rotating the polarization to align with the axes of anisotropic nanoparticles, orientational information can be extracted, giving rise to the nature of their local microenvironment.[4–7] Notably, polarimetric imaging of each individual nanoparticle has the potential to ascertain the precise spatial position (nm) of each constituent nanoparticle within a heterogeneous distribution. However, previous implementations utilize mechanical approaches in order to rotate the polarization.[8,9] Thus, resulting images are prone to beam deviation errors due to inherent mechanical and manufacturing limitations (surface defects, mechanical wobble, etc.).[10] While image processing can reduce beam deviation errors, we show these corrections are not sufficient at the sub-pixel scale to accurately correct spatial positions of individual nanoparticles.

In this paper, we describe a spatially precise, voltage-tunable nano-imaging system for direct observation of polarization-sensitive nanoparticles. Specifically, we integrate a voltage-tunable imaging variable polarizer (voltage-tunable IVP) with optical microscopy (darkfield), to stably image individual, polarization-sensitive nanoparticles. Here, voltage (Fig.1 (a)), rather than mechanical rotation (Fig. 1 (b)), is used to dynamically tune the transmission polarization angle and eliminate beam deviation errors. We demonstrate that the our nano-imaging system can achieve spatially stable and reproducible polarimetric images of nanoparticles with less than 30 nm beam deviation compared to conventional setups using mechanically rotated polarizers with larger than 1 μm beam deviation.

Nanoscale Imaging, Sensing, and Actuation for Biomedical Applications XV, edited by Alexander N. Cartwright, Dan V. Nicolau, Dror Fixler, Proc. of SPIE Vol. 10506, 105060F · © 2018 SPIE
CCC code: 1605-7422/18/$18 · doi: 10.1117/12.2289143

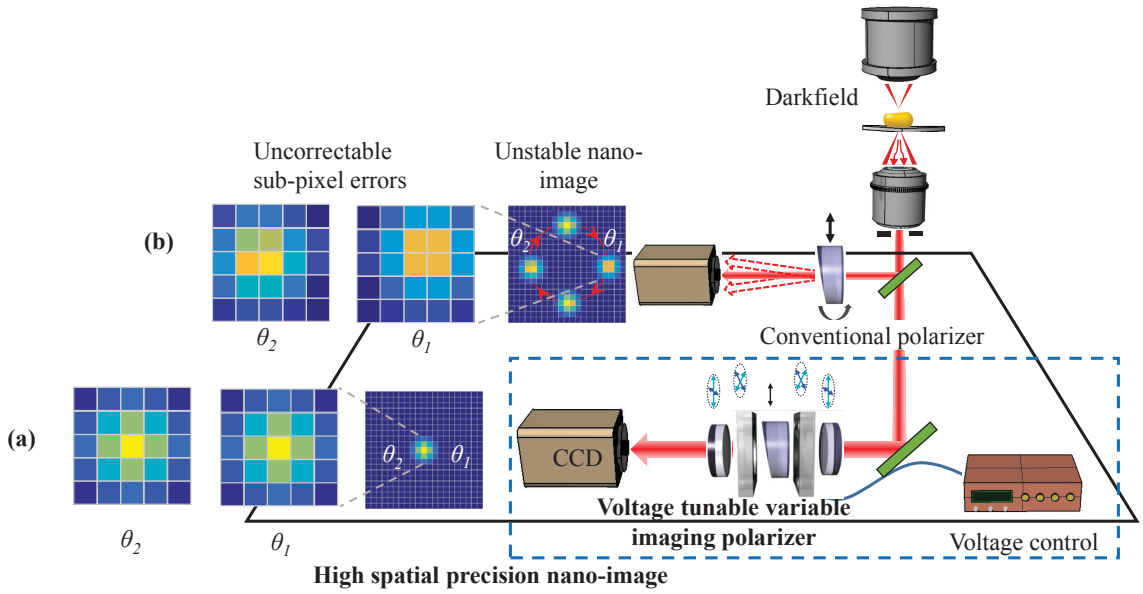

Figure. 1. Concept of high precision polarimetric nano-imaging by voltage-tunable imaging variable polarizer (IVP) compared to unstable imaging by mechanically rotated polarizer. (a) Voltage-tunable IVP: The polarimetric nano-imaging system integrates optical microscopy (darkfield) with a voltage-tunable IVP, resulting in spatially accurate polarimetric images of nanoparticles during the rotation of the polarizer (from θ_1 to θ_2), as shown in the foreground. **(b) Mechanically rotated polarizer:** As a comparison, a typical conventional imaging setup involving a mechanically rotated linear polarizer is depicted in the background, which results in unstable beam deviation errors (*i.e.*, image shift) and uncorrectable sub-pixel errors.

2. THEORY

In polarimetric nano-imaging, the beam deviation (Δl) caused by mechanical rotation of conventional polarizer can be quantified as

$$\Delta l = r[(\cos\theta - \cos\theta_0)^2 + (\sin\theta - \sin\theta_0)^2]^{1/2}, \tag{1}$$

where θ is the rotation angle of the polarizer, ($r\cos\theta_0$, $r\sin\theta_0$) and ($r\cos\theta$, $r\sin\theta$) are the spatial coordinates of the nanoparticle image before and after rotation of the polarizer. The spatial position difference before and after rotation arises from inevitable manufacturing defects (surface planarity, etc.) For an optical element, the two surfaces are not perfectly parallel to each other (Fig. 2), which is described as non-parallelism (with non-parallel angle α). During mechanical rotation, the rotation plane of the optical element often does not coincide with the optical element, causing the beam to shift (wobble). We believe that non-parallelism is the major contributor to the beam deviation. The beam deviation traces out a circular pattern due to the rotation symmetry of the linear polarizer. Therefore, given the polarizer refractive index n and distance between the CCD and the polarizer D, the radius of the circle is

$$r = D\alpha(n-1). \tag{2}$$

Substituting Eq. (2) into Eq. (1), the beam deviation can be expressed as

$$\Delta l = D\alpha(n-1)[(\cos\theta - \cos\theta_0)^2 + (\sin\theta - \sin\theta_0)^2]^{1/2}. \tag{3}$$

If we assume typical numbers for D, α, and n are 50 mm, 5 arcsec and 1.45 respectively, then a full rotation of the polarizer will result in the beam image tracing out a ~1.1 μm diameter circle at the CCD imaging plane (Fig. 2 (c)). When imaging polarization-sensitive nanoparticles, these beam deviation errors will cause a significant intensity error in the imaging plane which cannot be fully corrected beyond the pixel limit by image processing.

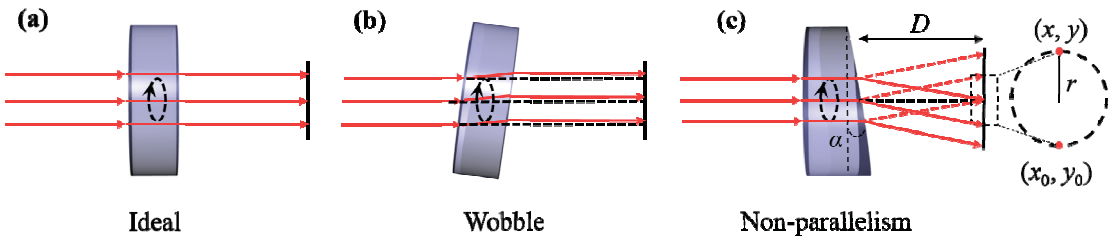

Figure 2. Beam deviation error as a result of wobble and non-parallelism. (a) Ideal case: For perfectly parallel surfaces, no beam deviation occurs after the rotation of the polarizer. **(b) Wobble:** Beam deviation due to the wobble by mechanical rotation. **(c) Non-parallelism:** Beam deviation due to the non-parallelism of the polarizer. *D* represents the distance between polarizer and the imaging plane; *r* is the radius of the traced circle; α is the angle between two non-parallel surfaces of the polarizer.

Conversely, liquid crystal retarders combined with waveplates can operate as a voltage-tunable variable polarizer, enabling tuning of transmission polarization angles without mechanical rotation. By integrating our voltage-tunable IVP into optical microscopy (darkfield), here, we demonstrate a high spatial precision polarimetric system for polarization-sensitive nanoparticle imaging.

3. EXPERIMENTAL METHODS

We use a gold nanorod to represent polarization-sensitive nanoparticles due to its high polarization sensitivity, high photostability and large scattering cross-section. The image target was prepared by conjugating single nanorods to a self-assembled monolayer (SAM) on a glass substrate.[11,12] The glass slide was first heated in the oven at 60 °C overnight to remove water content in the slide. After heating, the slide was then plasma treated for 30 seconds and immersed in 1.64% 3-Aminopropyl triethoxysilane (APTES)/ethanol solution to incubate for 24 hours. After incubation, the slide was washed with ethanol to remove excess APTES and then baked in the oven at 120 °C for 3 hours. A solution of gold nanorods was prepared by adding 1 mL of stock gold nanorods (absorbance of 1, peak wavelength of 802 nm) to 17.5 mL of DI water. After baking, the slide was immersed in this solution containing nanorods, creating a SAM-nanorod sample.

The voltage-tunable IVP consisted of two quarter waveplates, two liquid crystal retarders (LC #1 and LC #2) and one linear polarizer mounted in series. The SAM-nanorod sample was imaged by combining the voltage-tunable IVP with a dark-field microscope (IX73, Olympus) equipped with a dry condenser (U-DCD, Olympus), a 50x dark-field compatible objective (LMPLFLN50XBD) and a CCD camera (ORCA II, Hamamatsu). The voltage-tunable IVP was tuned by manually changing the voltages (2 kHz square wave) using a 2-channel function generator (AFG 2225, Instek). If both the LC #1 and LC #2 have the same retardation δ, the transmission polarization angles of the voltage-tunable IVP can be rotated by δ/2.[13] To avoid depolarization effects at the sample plane,[14] polarization was modulated by the voltage-tunable IVP at the detection path instead of the excitation path. For performance comparison with conventional mechanical systems, a linear polarizer (LPVISE200-A, Thorlabs) was placed between the output of the microscope and the camera, and then manually rotated. In both cases, the CCD camera was placed ~50 mm away from the optical elements. Finally, the locations of nanorods on the images were determined using a Laplacian of Gaussian filter (TrackMate, ImageJ Fiji).[15]

4. RESULTS & DISCUSSION

The performance of the voltage-tunable IVP nano-imaging system was characterized in two aspects, namely, imaging stability and polarization information accuracy in the spatial domain. For analysis, three nanorods (labelled as #1, #2, and #3) within the SAM-nanorod sample were selected, imaged and tracked. It can be seen that when using a mechanically rotated polarizer, the nanorod images followed a circular cyan trajectory (Fig. 3 (a)). Conversely, the images were stable in the case of voltage-tunable IVP, evidenced by the straight red track (Fig. 3 (b)).

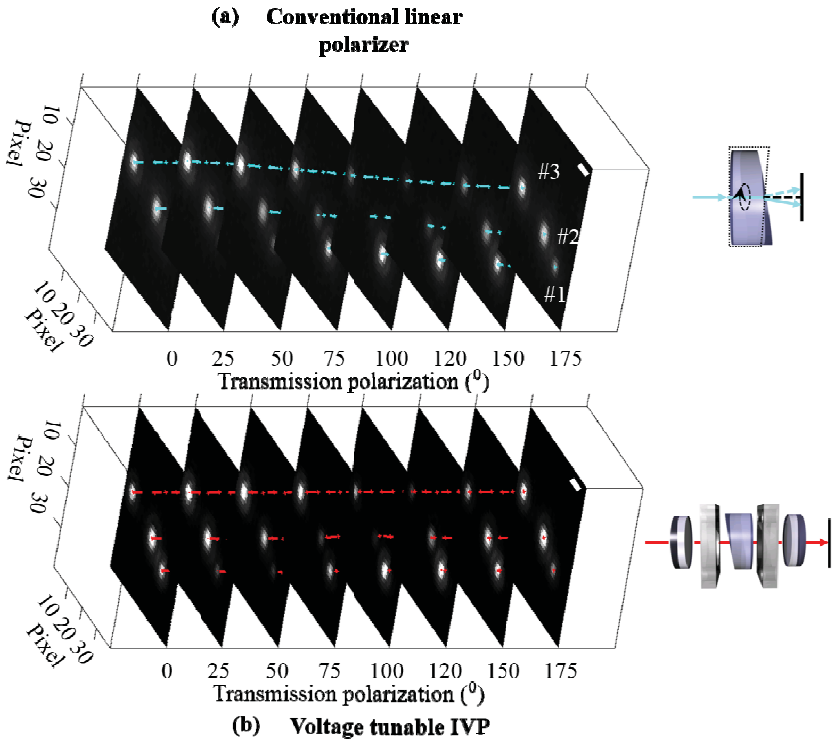

Figure 3. Voltage-tunable IVP suppresses spatial image shift by direct observation. Three nanorods were selected and imaged using a mechanically rotated polarizer and the voltage-tunable IVP with a polarization interval of 5°. Beam deviations of the three representative nanorods were tracked. **(a) Mechanically rotated polarizer** (cyan line). **(b) Voltage-tunable IVP** (red line). The scale bars are 1 μm.

Spatial stability was further quantitatively characterized in Fig. 4 where a single nanorod was tracked to analyze its relative image shift with respect to the transmission polarization angles using both the voltage-tunable IVP and mechanically rotated polarizer. The transmission polarization direction was changed from 0° to 175° in 5° increments. The tuning voltages are shown as a purple line (LC #1) and an orange line (LC #2). The square dots represent the mechanically rotated polarizer. Mechanical rotation of the polarization direction by 175° reached a maximum shift of ~ 1300 nm, matching reasonably close to theoretical calculations and fitting well with a sinusoidal function predicted in Eq. (3). Conversely, the relative image shift of the voltage-tunable IVP reached a maximum shift of ~30 nm (triangle dots, red line). We believe this remaining shift is largely due to vibrations from the surroundings and can be further reduced by employing a more stable imaging environment and faster voltage-tunable IVP tuning speed in the future.

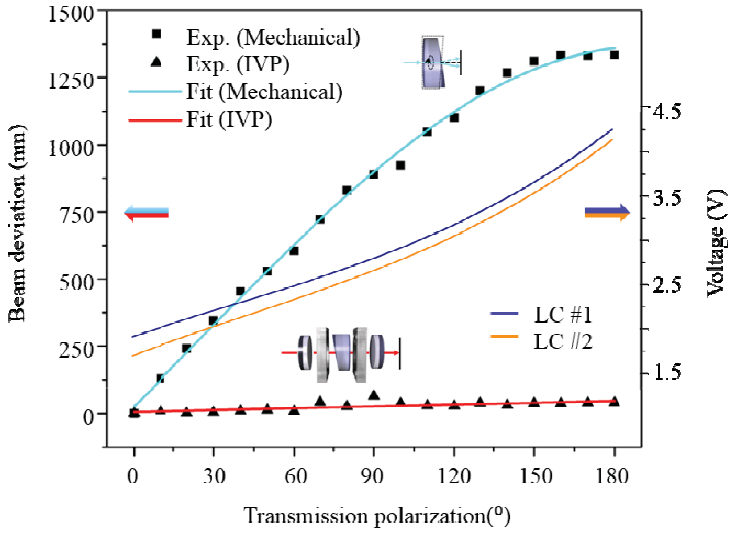

Figure 4. Voltage-tunable IVP suppresses spatial image shift by quantitative analysis. The relative beam deviation (nm) for a single nanorod was calculated and plotted for both the mechanically rotated polarizer (square dots, cyan line, fitted to a sinusoidal function), and the voltage-tunable IVP (triangle dots, red line, fitted to a linear function). The voltages used to tune the IVP for both liquid crystal retarders (purple for LC #1 and orange for LC #2) were plotted with respect to the same polarization directions.

Having demonstrated the spatial stability of the voltage-tunable IVP imaging system, we then investigated the polarization information accuracy in the spatial domain in terms of the beam deviation error. Beam deviation error refers to the inherent error of the pixel intensity when the image is shifted across pixels. This is fundamentally a result of intensity sharing between two neighboring pixels (illustrated in Fig. 1 (b)). The beam deviation error is defined as the normalized root-mean-square deviation (RMSD) of the intensity when fitted to a sinusoidal function, as shown in Eq. (4).

$$\mathrm{RMSD}\ (i,j) = \frac{1}{I_{e,\max}(i,j) - I_{e,\min}(i,j)} \sqrt{\frac{\sum_{m=1}^{N} (I_{e,m}(i,j) - I_{s,m}(i,j))^2}{N}}, \tag{4}$$

where N is the number of frames (each frame is taken at one polarization direction), I_e is the experimental value of the intensity, I_s is the theoretical value fitted to a sinusoidal function (which contains the orientation information of the nanorod), and $I_{e,\max}$ and $I_{e,\min}$ are the maximum and minimum intensities at pixel (i, j) over all polarization directions, respectively. For characterization, two nanorods were selected and labeled i and ii respectively (Fig. 5 (a)). The nanorods were imaged by tuning the transmission polarization from 0° to 175° in 5° increments. Three representative images at 50°, 100° and 150° are displayed for both the voltage-tunable IVP (Fig. 5 (c)) and the mechanically rotated polarizer (Fig. 5 (b)). In the latter case, the nanorod images were shifted several pixels away from their original positions at 0°, as indicated by the red dashed line in the image. For both nanorods, a small region-of-interest (5 x 5 pixels) from the beam center was cropped and analyzed for their RMSD. Overall, the voltage-tunable IVP imaging system generated consistently smaller RMSD values compared to conventional methods, and therefore can obtain more accurate polarization information in the spatial domain.

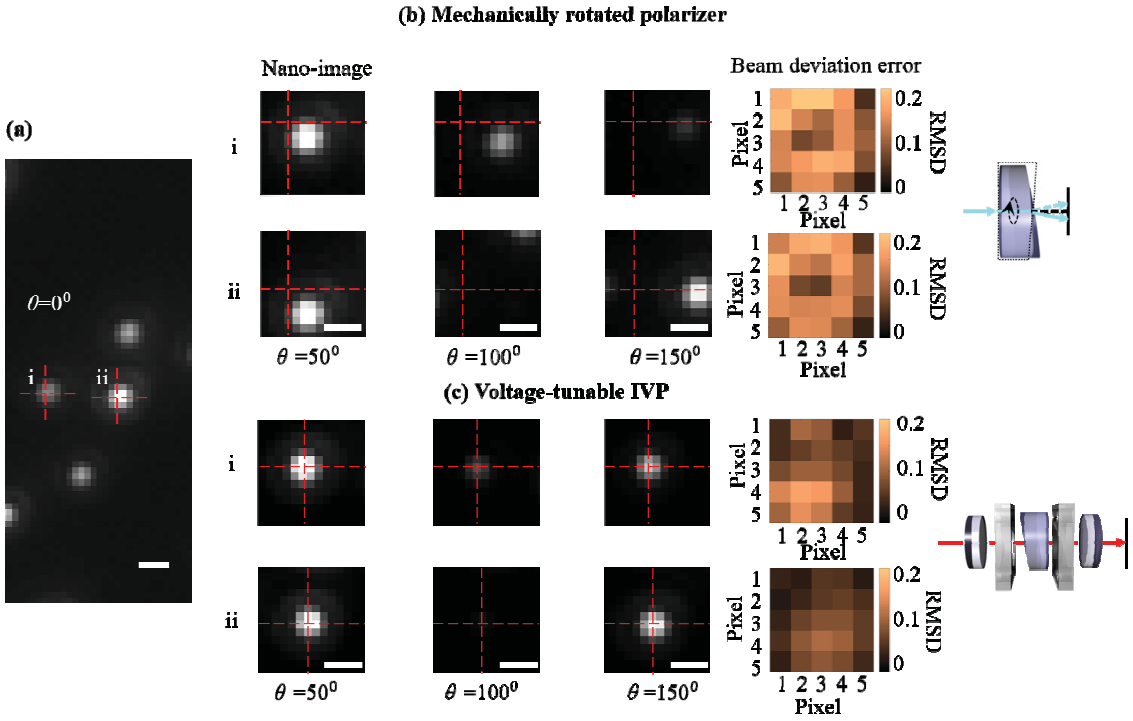

Figure 5. Voltage-tunable IVP enables spatial stability beyond the pixel limit. (a) Nano-image at 0^0 polarization: Two single gold nanorods (labeled i, and ii) were imaged using both the voltage-tunable IVP and the mechanically rotated polarizer. **(b) Nano-images at 50^0, 100^0 and 150^0 for mechanically rotated polarizer and beam deviation errors (RMSD):** The red dashed lines indicate the center pixel at 0^0 transmission polarization. Both nanorod i and ii were shifted away from their original locations. For each nanorod, the intensity of each pixel was fitted to a sinusoidal function and the beam deviation error was calculated in terms of the normalized root-mean-square deviation (RMSD) between the experimental and fitted values**. (c) Nano-images at 50^0, 100^0 and 150^0 for voltage-tunable IVP and beam deviation errors (RMSD):** No image shift was observed for the voltage-tunable IVP. The red dashed lines indicate the center pixel at 0^0. For each nanorod, the RMSD was calculated using the same method as **(b)**. Scale bars are 1 μm.

5. CONCLUSION

To summarize, we have demonstrated a voltage-tunable nano-polarimetric imaging system capable of high precision and high polarization information accuracy in the spatial domain. Voltage, instead of mechanical rotation, is used to alter the transmission polarization direction, thereby eliminating any spatial and polarization information errors, enabling observation of polarization-sensitive nanoparticles, and achieving spatial resolution beyond the diffraction limit.

REFERENCE

[1] Olson, J., Dominguez-Medina, S., Hoggard, A., Wang, L.-Y., Chang, W.-S., and Link, S., "Optical characterization of single plasmonic nanoparticles," Chem. Soc. Rev. **44**(1), 40–57 (2015).

[2] Sönnichsen, C., Franzl, T., Wilk, T., von Plessen, G., Feldmann, J., Wilson, O., and Mulvaney, P., "Drastic reduction of plasmon damping in gold nanorods," Phys. Rev. Lett. **88**(7), 77402 (2002).

[3] Wang, G., Sun, W., Luo, Y., and Fang, N., "Resolving rotational motions of nano-objects in engineered environments and live cells with gold nanorods and differential Interference contrast microscopy," J. Am. Chem. Soc. **132**(46), 16417–16422 (2010).

[4] Perez-Juste, J., Rodriguez-Gonzalez, B., Mulvaney, P., and Liz-Marzan, L. M., "Optical control and patterning of gold-nanorod-poly(vinyl alcohol) nanocomposite films," Adv. Funct. Mater. **15**(7), 1065–1071 (2005).

[5] H. Wang, T. B. Huff, D. A. Zweifel, W. He, P. S. Low, A., and Wei, J. X., "In vitro and in vivo two-photon luminescence imaging of single gold nanorods," Proc. Natl. Acad **102**(44), 15752–15756 (2005).

[6] Huang, X., El-Sayed, I. H., Qian, W., and El-Sayed, M. A., "Cancer cells assemble and align gold nanorods conjugated to antibodies to produce highly enhanced, sharp, and polarized surface Raman spectra: A potential cancer diagnostic marker," Nano Lett. **7**(6), 1591–1597 (2007).

[7] Sönnichsen, C. and Alivisatos, A. P., "Gold nanorods as novel nonbleaching plasmon-based orientation sensors for polarized single-particle microscopy," Nano Lett. **5**(2), 301–304 (2005).

[8] Zijlstra, P. and Orrit, M., "Single metal nanoparticles: optical detection, spectroscopy and applications," Reports Prog. Phys. **74**(10), 106401 (2011).

[9] Nehl, C. L., Liao, H., and Hafner, J. H., "Optical properties of star-shaped gold nanoparticles," Nano Lett. **6**(4), 683–688 (2006).

[10] Møller, K. H. and Trabjerg, I., "Investigation of problems associated with infrared image detection using rotating polarizers," Infrared Phys. Technol. **46**(4), 351–354 (2005).

[11] Cao, C., Birtwell, S., Høgberg, J., Morgan, H., Wolff, A., and Bang, D., "Gold nanoparticles-coated SU-8 for sensitive fluorescence-based detections of DNA," Diagnostics **2**, 72–82 (2012).

[12] Sarkar, A. and Daniels-Race, T., "Electrophoretic deposition of carbon nanotubes on 3-amino-propyl-triethoxysilane (APTES) surface functionalized silicon substrates," Nanomaterials **3**, 272–288 (2013).

[13] Safrani, A. and Abdulhalim, I., "Liquid-crystal polarization rotator and a tunable polarizer," Opt. Lett. **34**(12), 1801–1803 (2009).

[14] Lassiter, J. B., Aizpurua, J., Hernandez, L. I., Brandl, D. W., Romero, I., Lal, S., Hafner, J. H., Nordlander, P., and Halas, N. J., "Close encounters between two nanoshells," Nano Lett. **8**(4), 1212–1218 (2008).

[15] Tinevez, J.-Y., Perry, N., Schindelin, J., Hoopes, G. M., Reynolds, G. D., Laplantine, E., Bednarek, S. Y., Shorte, S. L., and Eliceiri, K. W., "TrackMate: an open and extensible platform for single-particle tracking," Methods **115**, 80–90 (2017).